Topological wave energy harvesting in bistable lattices

Myungwon Hwang

Andres F. Arrieta

Purdue University, Department of Mechanical Engineering, West Lafayette, IN 47907, USA

E-mail: aarrieta@purdue.edu

July 2021

Abstract. In this paper, we present an input-independent energy harvesting mechanism exploiting topological waves. Transition waves in discrete bistable lattices entail energy radiation in the form of trailing phonons. We observe numerically and experimentally that the most dominant frequencies of these phonons are invariant to the details of the input excitations as long as transition waves are generated. Most of the phonon energy at each unit cell is clustered around a single invariant frequency, enabling input-independent resonant energy transduction. An electromagnetic conversion mechanism is implemented to demonstrate that bistable lattices behave as generators of fixed-frequency electrical sources upon transition wave propagation. The presented mechanism fundamentally breaks the link between the unit cell size and the metamaterial's operating frequencies, offering a broadband solution to energy harvesting, particularly robust for low-frequency input sources. We also investigate the effect of lattice discreteness on the energy harvesting potential, observing two performance gaps and a topological wave harvesting pass band where the potential for energy conversion increases almost monotonically. The observed frequency-invariant phonons are intrinsic to the discrete bistable lattices, enabling broadband energy harvesting to be an inherent metamaterial property.

Keywords: energy harvesting, transition waves, bistable lattices

1. Introduction

Energy harvesting promises to power small electronics and IoT devices. Utilizing vibrations and motion as a power source has received significant attention over the past two decades [1, 2, 3, 4]. Initial efforts focused on designing devices capable of significant power conversion leveraging linear [5, 6, 7] and nonlinear [8, 9, 10, 11] oscillations, revealing the crucial role of resonance as an efficient mechanism for energy harvesting. Since the vibration frequencies and levels vary vastly among the ambient sources [2, 12],

an extensive number of frequency tuning strategies have been explored. These strategies include adjusting the mechanical [13, 14, 15, 16] or electrical [17, 18, 19, 20, 21] components and varying the harvester geometries [22, 23]. More recently, metamaterials or material systems with engineered unit cells to produce unconventional properties have been explored as energy harvesters, exploiting band gaps [24], wave focusing [25, 26, 27], engineered defects [28, 29, 30, 31], metasurfaces [32, 33], and rainbow trapping in protected edge modes [34].

At the heart of both device- and metamaterial-based energy harvesting strategies lies the interplay between size and operating frequency. In energy harvesting devices, resonances are determined by the stiffness and mass of the vibrating structures so that the sizes are fundamentally constrained by the density law [35]. In metamaterials, both scattering [36] and local resonance-based [37] routes to achieve energy conversion are also intimately related to the unit cell size [Fig. 1(a)]. In both cases, this size dependence strongly limits the operating frequency conversion range, rendering energy harvesting from low-frequency inputs particularly challenging. Mechanisms such as frequency up-conversion [38, 39, 40] for devices and nonlinear dispersion [41, 42] for metamaterials are still limited by the fundamental relationship between size and effective bandwidth. Hence, practical implementation of motion-based energy harvesting for low-frequency and ultimately broadband applications calls for a fundamentally different dynamic mechanism that is not strongly governed by the input frequency. Recently, a phenomenon enabling energy exchange from a source (input) to a desired (output) frequencies has been established, leveraging the input-independent response of metamaterials sustaining transition waves [43, 44]. This type of solitary wave is triggered when an amplitude threshold is reached, regardless of the input nature, propagating unperturbed as quasi-particles through the metamaterial's constitutive lattice. This allows for harvesting energy from a wide variety of inputs without relying on resonant matching/tuning that makes conversion from low-frequency bands especially challenging.

We present a mechanism exploiting the strong nonlinear response of transition waves for realizing input-independent energy harvesting as a metamaterial property. In the sense that transition waves are also referred to as topological waves, we define our input-independent energy conversion mechanism as topological wave energy harvesting. Our mechanism leverages radiating waves (phonons) induced as transition waves propagate in discrete bistable lattices [45, 46, 47] to convert energy from the input. Crucially, the frequencies of these phonons are fixed by the lattice design while being completely independent of the input triggering the transition waves. Thus, this mechanism breaks the strong connection between the device/unit cell size and the harvesting bandwidth. With the integrated electromagnetic transduction mechanism, the vibration energy of the radiated phonons can be converted into fixed-frequency electrical sources, offering a new route to broadband energy harvesting. We further unveil that controlling the constitutive lattice's discreteness yields a topological wave energy harvesting band in which transition waves induce transducible phonons without

losing their ability to propagate. This energy harvesting band gives a concrete metric for the lattices design. Our topological wave harvesting metamaterials enable the embedding of power conversion into material systems, opening a robust avenue for powering electronics and IoT devices even from very low-frequency sources.

2. Fundamental dynamics in bistable lattices

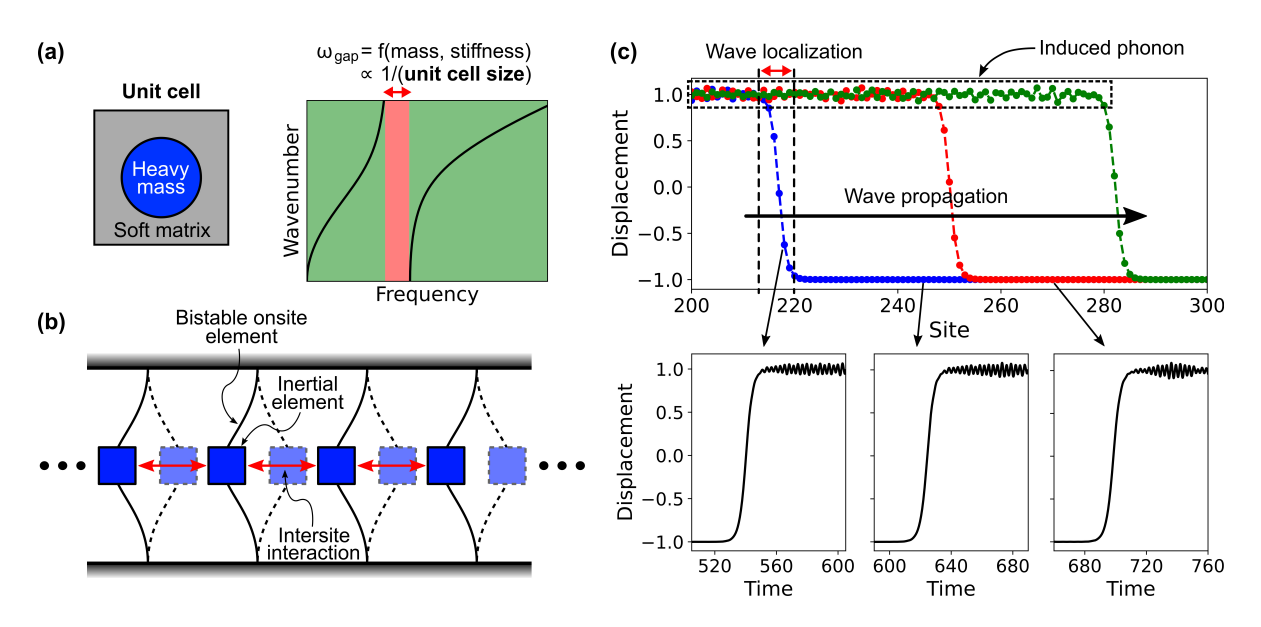


Figure 1. (a) Illustration of the unit cell size dependence of the operating frequencies in metamaterials. (b) Generic bistable lattice, showing the key components. (c) Typical propagation of a transition wave in a discrete bistable lattice.

The introduced topological wave energy harvesting mechanism can be obtained from metamaterials with a bistable microstructure (henceforth referred to as bistable lattices), which sustain transition waves. Generically, bistable lattices can be obtained from 1) bistable potentials acting directly on the constitutive masses (on-site type) [48, 49, 50, 51] and 2) from bistable forces linking neighboring masses (inter-site type) [52, 53]. Throughout this work, we will focus on the on-site bistable lattices dropping the distinction for simplicity. Figure 1(b) illustrates the key components the considered bistable lattices, where the neighboring masses are bound by a form of inter-site force. The most crucial compositional feature is the bistability of the on-site element, which allows two (or more) globally stable configurations. Changes between these globally stable configurations are promoted by transition waves, also commonly called topological solitary waves [54]. A typical propagation of a transition wave in a discrete bistable lattice and the corresponding time responses at individual sites are shown in Fig. 1(c), revealing a highly localized waveform that spans between two topologically different stable states. The stiffness ratio between the on-site and inter-site elements determines the lattice discreteness, a notable byproduct of which is the radiation of energy in the form of induced vibration, or phonons, following the transition wave.

A phonon is an elementary wave mode in phononic crystals [55, 56] and resonant-based metamaterials [37, 57]. Previous works have investigated the radiation of phonons from propagating transition waves in discrete bistable lattices [45, 46, 58, 59, 60, 61]. Since transition waves can be triggered independently of the input excitations [43], the careful matching between the input and harvester dynamics ubiquitous in resonance-based energy harvesting becomes insignificant. In the sense that resonance is intimately related to the size of the substructure (for devices) and unit cell (for metamaterials), the proposed exploitation of radiating phonons from propagating transition waves breaks this strong scale dependence [see Fig. 1(a)], opening a new mechanism for energy harvesting. In this paper, we characterize the dynamics of the induced phonons in discrete bistable lattices and seek a strategy to harvest their energy in a physical system.

3. Bistable lattice model

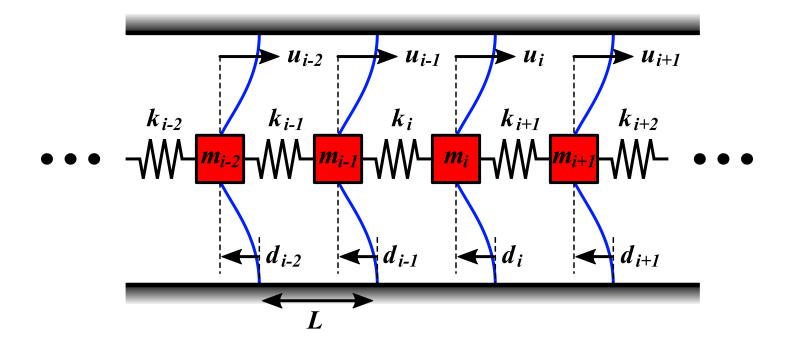


Figure 2. Schematics of the bistable lattice model for the numerical simulations.

We conduct numerical simulations to investigate the characteristic behaviors of the induced phonons and leverage the discovered dynamics for energy harvesting. To that end, we keep only the essential components for the numerical lattice model and use a minimal characterization for each component, as introduced in several previous studies [62, 49, 43, 63, 64]. Figure 2 shows the schematic diagram of the bistable lattice. m_i is the point mass of the i^{th} unit cell that is connected to the neighboring masses by a linear inter-site spring with stiffness k_i to the left and spring with stiffness k_{i+1} to the right. The unit cells are separated by a distance L although this distance does not appear explicitly in the governing equation to follow. The bistable onsite potential energy is designed to be symmetric to allow both the compressive and tensile types of the transition waves [65] and is approximated by a 4th-order polynomial $\phi_{\text{onsite}}(\Delta) = \frac{B}{4}\Delta^4 - \frac{Bd_i^2}{2}\Delta^2$, where Δ is the deflection from the unstable equilibrium, $\pm d_i$'s are the stable equilibria at i^{th} unit cell, and the constant B controls the magnitude. In addition, dissipation is unavoidable in physical systems, which is modeled as velocity-proportional on-site damping with a coefficient b_i (not shown in Fig 2). Combining all the components together, we obtain the governing equation for the displacement u_i of

the i^{th} unit cell from its unstable equilibrium position as

$$m_i \ddot{u}_i + b_i \dot{u}_i + k_i (u_i - u_{i-1}) - k_{i+1} (u_{i+1} - u_i) + B u_i (u_i^2 - d_i^2) = 0, \tag{1}$$

where the overdot represents the differentiation with respect to time.

To reduce the number of parameters and obtain results in generic scalable forms, we nondimensionalize Eq. (1) as follows.

$$\bar{m}_i \bar{u}_i'' + \bar{b}_i \bar{u}_i' + \bar{k}_i (\bar{u}_i - \bar{u}_{i-1}) - \bar{k}_{i+1} (\bar{u}_{i+1} - \bar{u}_i) + \bar{B} \bar{u}_i (\bar{u}_i^2 - \bar{d}_i^2) = 0, \tag{2}$$

where the prime represents the differentiation with respect to nondimensional time \bar{t} , and the following nondimensionalizations are used:

$$\bar{t} = \frac{t}{T}, \ \bar{u}_i = \frac{u_i}{d_1}, \ T = \sqrt{\frac{m_1}{k_i}}, \ \bar{m}_i = \frac{m_i}{m_1}, \ \bar{b}_i = \frac{b_i}{\sqrt{m_1 k_1}}, \ \bar{k}_i = \frac{k_i}{k_1}, \ \bar{B} = \frac{Bd_1^2}{k_1}, \ \bar{d}_i = \frac{d_i}{d_1}.$$
 (3)

To allow stable propagation of transition waves in a physical system (i.e., a nonconservative system), we apply graded parameters in the propagation direction [65, 66]. Particularly, we use the following linear grading with a decrement ζ .

$$\bar{m}_i = 1 - (i-1)\zeta, \quad \bar{b}_i = \bar{b}_1[1 - (i-1)\zeta], \quad \bar{k}_i = 1 - (i-1)\zeta, \quad \bar{d}_i = \sqrt{1 - (i-1)\zeta}.$$
 (4)

This choice of grading has the benefit of keeping the discreteness level nearly constant throughout the lattice—since both on-site stiffness $(2\bar{B}\bar{d}_i^2)$ and inter-site stiffness (\bar{k}_i) change with the same proportionality $1-(i-1)\zeta$, their ratio is kept constant. In its final form, the nondimensionalized governing equation becomes unique with the specification of only three parameters $(\bar{B}, \zeta, \text{ and } \bar{b}_1)$. As the baseline design, we start with $\bar{B}=1.7$. We choose $\zeta=0.01$ so that the lattice can be made sufficiently long (90 unit cells long in our simulation environment) to be considered as a metamaterial. Also, very light damping $(\bar{b}_1=0.05)$ is applied to attenuate phonons in the length of the lattice. All the numerical simulations in this paper are performed with an in-house Fortran solver, which has been thoroughly validated for general systems with bistable microstructures [67].

4. Phonon frequency invariance

To analyze the dependence of the phonon responses on the excitation conditions, we first excite the bistable lattice with impulsive and quasi-static loads. To allow spontaneous snap-through transition of the first unit cell upon reaching a critical snapping distance, we apply an input force to the first unit cell in the following form. For a compressive load $F_{\text{comp}}(\bar{t})$,

$$F_{\text{comp}}(\bar{t}) = \begin{cases} 0 & \text{for } l(\bar{t}) < \bar{u}_1(\bar{t}) \\ k_{\text{in}}[l(\bar{t}) - \bar{u}_1(\bar{t})] & \text{for } l(\bar{t}) \ge \bar{u}_1(\bar{t}), \end{cases}$$
(5)

where $k_{\rm in}$ and $l(\bar{t})$ are the stiffness of a fictitious spring and the applied (nondimensional) displacement from the unstable equilibrium of the first unit cell in the direction of the

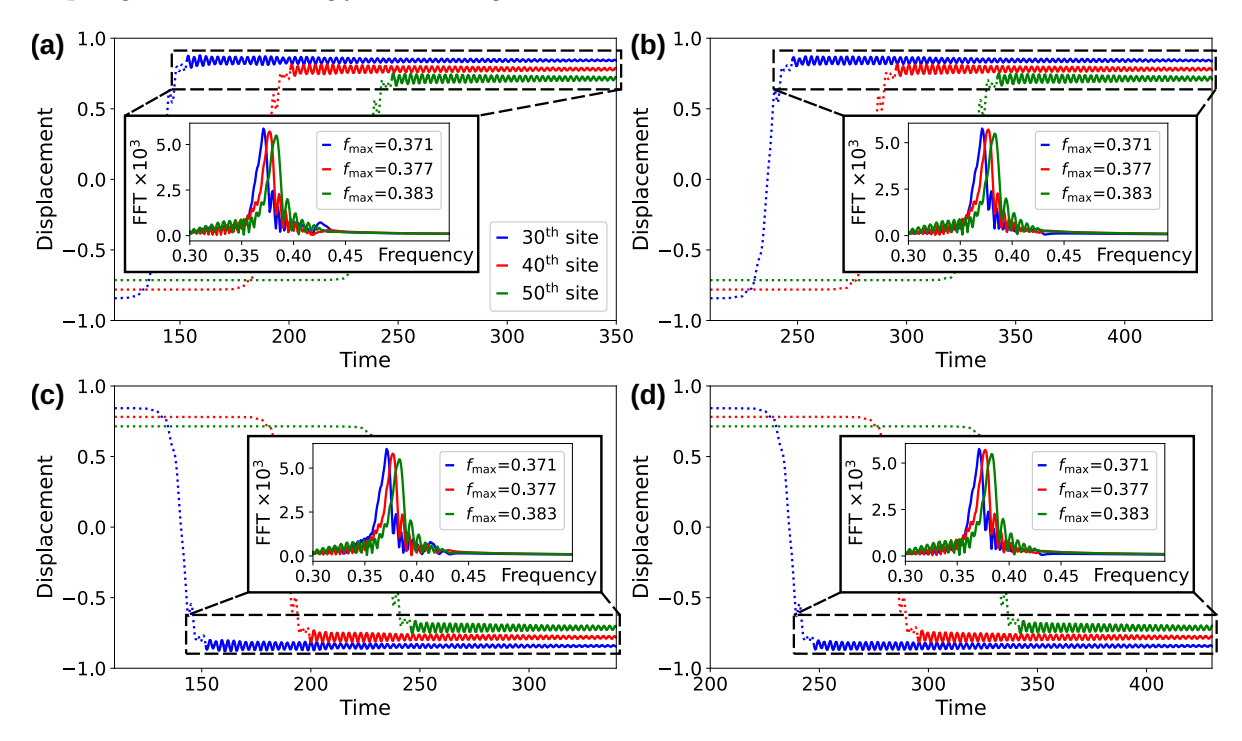


Figure 3. Time displacements of the 30^{th} , 40^{th} , and 50^{th} unit cells under (a) impulsive compressive, (b) quasi-static compressive, (c) impulsive tensile, and (d) quasi-static tensile loads, respectively. In the insets are the corresponding frequency spectra and the most dominant frequencies f_{max} .

lattice. A tensile load $F_{\text{tens}}(\bar{t})$ is applied similarly but in the opposite conditions:

$$F_{\text{tens}}(\bar{t}) = \begin{cases} k_{\text{in}}[l(\bar{t}) - \bar{u}_1(\bar{t})] & \text{for } l(\bar{t}) \leq \bar{u}_1(\bar{t}) \\ 0 & \text{for } l(\bar{t}) > \bar{u}_1(\bar{t}). \end{cases}$$
(6)

The intensity of the excitation is controlled by the time duration of the force application. For the compressive (tensile) loads, $l(\bar{t})$ is applied from -1.1 (1.1) to 0.95 (-0.95) with $k_{\rm in}=10$ over 1 time unit for an impulsive input while the same distance is applied over 100 time units for a quasi-static input.

Figure 3 shows the displacements of selected unit cells (30th, 40th, and 50th) under impulsive and quasi-static loads in both directions, which are large enough to trigger transition waves. The analyzed unit cells are sufficiently within the lattice to focus on the metamaterial property and minimize any significant boundary effects. As expected for a typical discrete lattice supporting transition waves, we observe radiation of energy in the form of induced phonons (indicated in solid lines) trailing the snap-through transitions. The frequency spectra of these phonons are analyzed by taking Fast Fourier Transform (FFT) using fftpack module from Python's SciPy library. For every frequency response in the numerical investigation, the FFT is performed on 2000 time units of the velocity response, corresponding to the induced phonon, at the sampling rate of 100 without applying a window function. The velocity data are either trimmed when the induced phonon lasts more than 2000 time units or padded with zeros if it lasts shorter than

2000 time units so that the frequency resolution is always kept at 0.0005. The response's most dominant frequency at each unit cell is indicated in the inset as f_{max} . This analysis shows that the dominant frequency of the radiated phonon at each site remains invariant regardless of the input's type (compression or rarefaction) and intensity. This frequency invariance, which works in both excitation directions, implies a strong potential for broadband energy harvesting provided that a transduction mechanism is integrated at each unit cell. This would allow for the phonon's energy at each unit cell to be effectively harvested with only a single circuit design optimally tuned for this invariant phonon frequency. Concretely, this allows for ensuring resonant transduction from phonons as long as transition waves are triggered within the lattice, independently from the inputs' nature. Consequently, the proposed topological wave energy harvesting mechanism yields a broad and size-independent conversion bandwidth.

5. Induced phonons under harmonic excitations

The invariant frequency response under a single transition wave also leads to the possibility for input-independent energy harvesting under harmonic excitations. We explore this regime by exciting the lattice with sinusoidal inputs with a displacement amplitude of 1.1 at various input frequencies $\bar{f}_{\rm in}$. Figure 4(a) shows an example response under a low-frequency input ($\bar{f}_{\rm in}$ =0.0016) such that the induced phonons have enough time to dissipate before the next snap-through transition occurs. The most dominant frequencies of the phonons indicated in the inset are almost identical to the invariant frequencies obtained under a single transmission of a transition wave, showing the repeatability of the invariant frequency responses at every half cycle.

As the input frequency is increased, the duration of the induced phonons is shortened by the faster transition wave generation rate. As a result, the frequency responses can be affected by the interactions with the snap-through transitions and their own reflections. We categorize this kind of input frequencies as a high frequency in this paper. One example case under an input frequency of 0.007 is shown in Fig. 4(b), where the time responses of the phonons are different for each half cycle, and the dominant frequencies of the phonons are slightly shifted from the inherent system frequencies determined by the lattice design. Nevertheless, the fluctuations are within 10% of the system frequencies (Q=10 if resonant transduction is set to occur at these values), ensuring a close to optimal transduction of the phonon energy.

When the input frequency becomes very high such that propagating and newly generated transition waves interact, the snap-through transitions away from the excitation site occur at random rates [44] as shown in the example response under an input frequency of 0.02 [Fig. 4(c)]. Especially when the transition wave generation is delayed for a long period, the bistable lattice sectionally behaves like a linear system; thus, the induced phonons are perturbed by other kinds of waves, such as local reflections, pinned transition waves, and their interactions. Even at these very high frequency inputs, we can expect appreciable power generation since the phonon

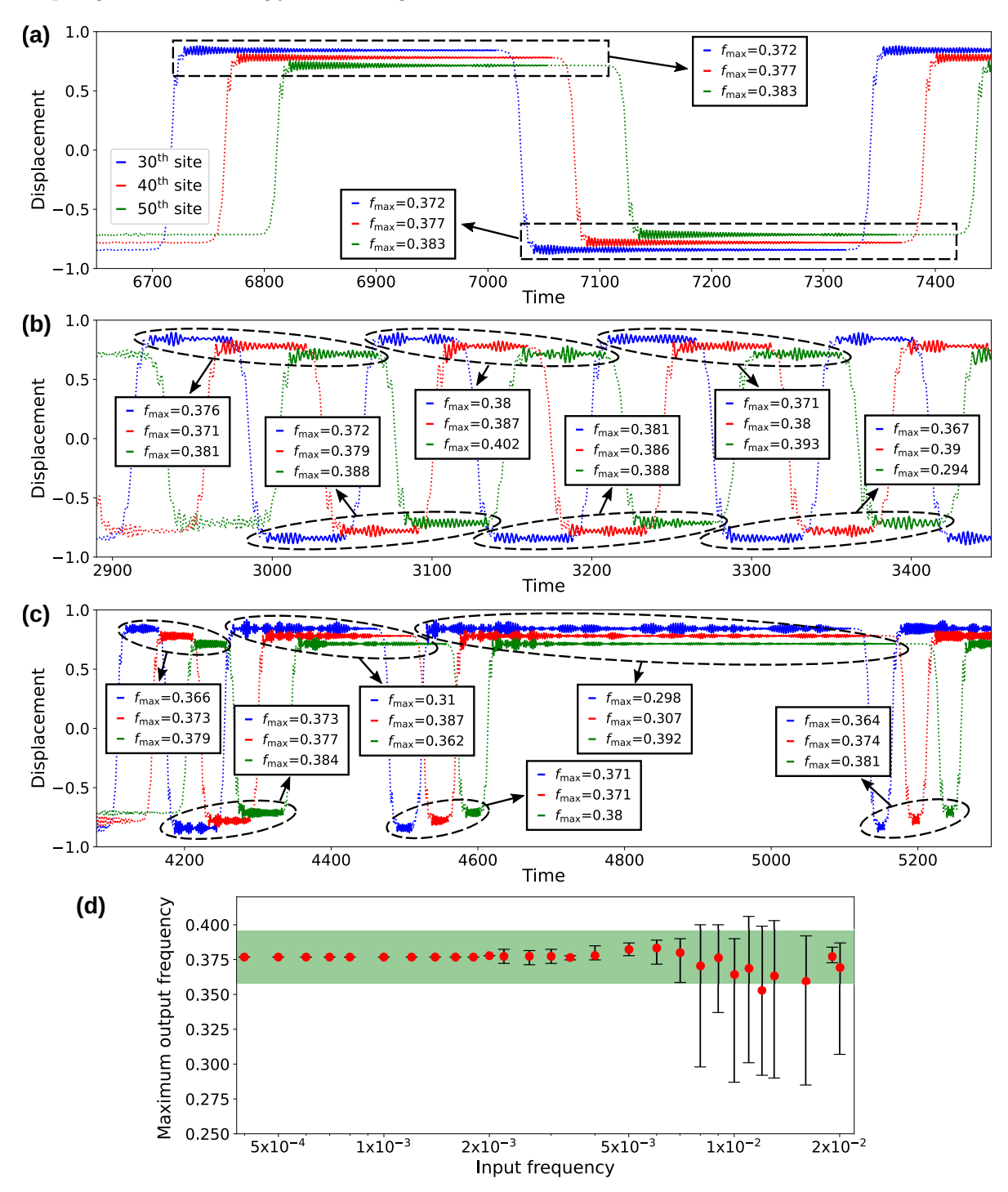


Figure 4. Time displacements of the 30th, 40th, and 50nd unit cells under displacement inputs with (a) low (0.0015), (b) high (0.007), and (c) very high (0.02) frequencies. (d) Output frequency diagram, showing the most dominant frequency of the 40th unit cell on average as a function of the input frequency.

frequencies are still invariant for many other time periods. However, we will exclude these frequency cases from the operating frequency band from our analysis since we cannot reliably transduce the phonon energy all the time. We investigate the input frequency dependence on the dominant output frequencies of the phonons by taking the $40^{\rm th}$ unit cell's most dominant phonon frequencies averaged over ten measurements while holding the displacement amplitude constant at 1.1 [Fig. 4(d)]. The associated error bars show the distributions of the dominant frequencies from different measurements, and the green shaded region indicates the $\pm 5\%$ bound of the inherent system frequency (0.377). Regardless of the input frequency, the dominant output frequency remains within this bound up to $\bar{f}_{\rm in}$ =0.007, rendering the transition wave-induced phonons fully independent of the excitation frequencies. This response invariance (encompassing impulsive, quasi-static, and harmonic sources) embodies the mechanism breaking the connection between operating bandwidth and unit cell size that impedes the broad implementation of energy harvesting. In particular, the lack of phonon frequency fluctuations over the frequency band $\bar{f}_{\rm in} < 0.002$ ensures that the input-independent conversion is extremely effective for low-frequency sources. This provides a route to low-frequency harvesting applications which have remained a major challenge for linear and weakly nonlinear metamaterials.

Bistable lattices are highly scalable for their simple periodic arrangement and due to the geometric nature of the on-site potential implementations using arches [68, 49] or domes [69]. As long as the discrete nature of the bistable lattice is kept, the lattices can be designed to operate over different frequency ranges. The physical frequency and the nondimensional frequency are related by $f = \bar{f}/T = \sqrt{k_1/m_1}\bar{f}$. For example, if the unit cells were made in the size similar to those of our experimental demonstrator to follow (Fig. A1), the operating input frequency range for topological wave energy harvesting would be approximately from 0 Hz to 1 Hz. The operating bandwidth can be easily tuned to encompass orders of magnitude higher frequencies with smaller unit cell designs. Experimental realization of the lattices with such smaller unit cells only requires micro- or nano-scale manufacturing technology, which is already available as demonstrated in many architectured materials [70, 71, 72, 73].

6. Discreteness effect on harvesting capability

Lattice discreteness is a necessary characteristic to obtain the presence of frequency-invariant phonons. Thus, we investigate the role of lattice discreteness to enhance the topological wave energy harvesting capabilities of the considered bistable metamaterials. We use the ratio of on-site element and inter-site element to introduce variation in lattice discreteness. Specifically, we define lattice discreteness as the ratio between $\bar{B}\bar{d}_1^2$ and \bar{k}_1 , which is simply \bar{B} . We leverage numerical simulations for various values of \bar{B} to show the effect of the lattice discreteness on the energy harvesting potential and analyze the phonon energy that can be resonantly transduced. To this end, we keep the input condition and all other lattice parameters the same as those of the quasi-static compressive case in Sec. 4.

When transforming quantities in the time domain into those in the frequency domain, the transformed quantities can be manipulated to represent the actual energy

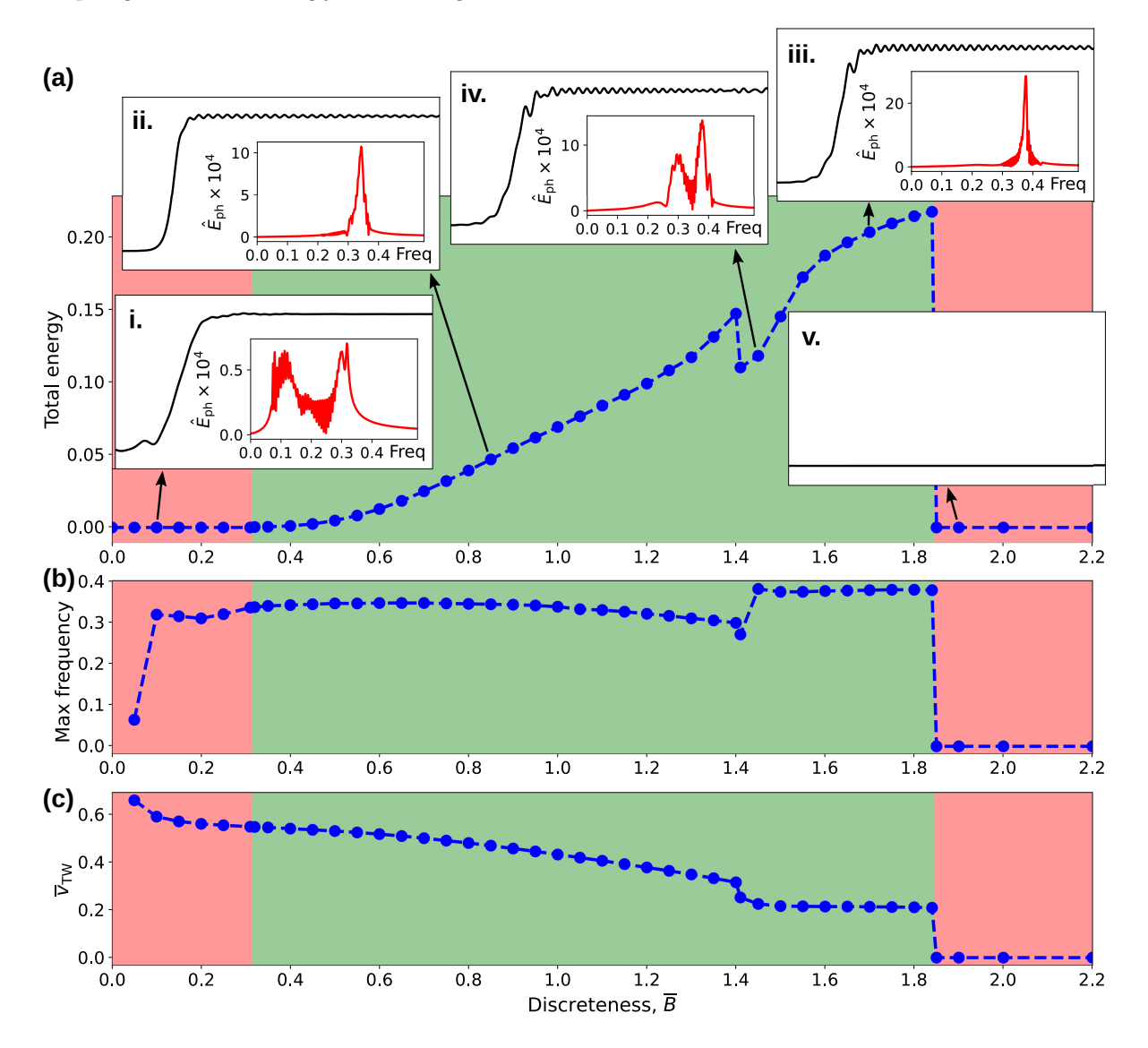


Figure 5. (a) Topological wave energy harvesting potential, (b) dominant phonon frequency at 40th site, and (c) average propagation speed of the transition wave as a function of lattice discreteness. The green (red) shaded region indicates that the phonon energy can (not) be resonantly transduced with our invariant energy harvesting mechanism. In the insets are the characteristic responses and energy spectral densities: (i) nearly continuous lattice yielding no transducible phonons, (ii) lightly discrete lattice generating frequency-invariant phonons, (iii) moderately discrete lattice yielding more energetic phonons, (iv) lattice in the transitional region between the light and moderate discreteness, and (v) highly discrete lattice destroying transition wave propagation.

associated with each frequency. From Parseval's theorem,

$$\sum_{n=0}^{N-1} |x_n|^2 \Delta t = \frac{1}{N} \sum_{k=0}^{N-1} |\hat{x}_k|^2 \frac{\Delta f}{\Delta f} \Delta t = \sum_{k=0}^{N-1} \frac{t_{\text{total}}^2}{N^2} |\hat{x}_k|^2 \Delta f, \tag{7}$$

where \hat{x}_k 's are the FFT of the discrete time signals x_n 's, N is the number of samples, Δt is the time step, Δf is the frequency step, and t_{total} is the total time of the signal. If

the quantity x_n were chosen as $\sqrt{b}\bar{u}_i'$, the summations on both sides of the equality sign should amount to the approximate time integral of the power dissipated at i^{th} unit cell, which is the total dissipated energy at that site. Therefore, $2|\hat{x}_n|^2t_{\text{total}}^2/N^2$ corresponds to the actual energy spectral density at each frequency. The multiplicative factor 2 is introduced since the amplitudes of the transformed quantities of a real-valued data set are split in half between the positive and negative frequencies.

Predicting the actual harvested energy would require involved analyses of coupled electromechanical equations and characterization of the circuit elements. However, it is natural to expect that more energy would be converted when more phonon energy is concentrated around a fixed frequency matched to the electrical impedance of the conversion circuit. Thus, instead of introducing an electrical model, we assume that the available phonon energy concentrated around the dominant phonon frequency can offer a qualitative measure of the energy harvesting potential.

The induced phonon energy available at each site for invariant harvesting can be obtained by the numerical integration of the energy spectral density between a small frequency range ($\pm 5\%$) about the maximum phonon frequency. Figure 5(a) summarizes the total phonon energy available between 30th and 49th sites, which can be invariantly transduced, as a function of the lattice discreteness. The ranges of the discreteness values yielding essentially zero transducible phonon energy are indicated in shaded red. Two such ranges can be identified, which we referred to as the lower and upper energy harvesting gaps, respectively. Between these gaps lies a discreteness value range offering identifiable dominant phonon frequencies. We refer to this range as the topological wave harvesting pass band.

Five representative responses at 40th site are plotted in the insets of Fig. 5(a) along with the corresponding energy spectral densities \hat{E}_{ph} of the phonons. When the bistable lattice approaches a continuum limit ($\bar{B} < 0.32$ for the given example lattice), the transition waves propagate without clearly identifiable induced phonons since the formation energy of the transition wave is essentially the same among the available transition wave configurations—this energy difference can be described by Peierls-Nabarro barrier [74, 75]. Although some fluctuations following a transition wave appear for a non-zero discreteness value in the lower gap, a single dominant phonon frequency cannot be readily identified, as shown in the inset (i). Since our harvesting mechanism relies on the generation of frequency-invariant phonons, we cannot achieve effective power conversion in nearly continuous bistable lattices. For a lightly discrete lattice, we start to observe phonons displaying single dominant peaks [inset (ii)]. Thus, most of their energy can be efficiently harvested. When the discreteness increases further toward the upper boundary of stable transition wave propagation, which we call moderately discrete, phonons with higher energy can be observed [inset (iii)]. The phonon energy increases almost monotonically with the lattice discreteness in the pass band. There is a slight dip for $1.4 < \overline{B} < 1.55$ since the dominant phonon frequency splits into two [inset (iv)], leaving only the portion of the phonon energy corresponding to the larger of the two frequencies available for the resonant transduction. We hypothesize the dip to occur due to the transition from one preferred wave mode to another. Figure 5(b) summarizes the most dominant frequency peaks of the phonons at 40^{th} site, which shows two different frequency branches in the pass band: the lower-frequency one corresponds to the lightly discrete lattice, and the other corresponds to the moderately discrete lattice. As expected, the transitional region between the two branches coincides with the discreteness range where the harvesting potential dip occurs. More in-depth investigation on the nature of each frequency branch will follow in a separate study. Finally, when the discreteness becomes too strong ($\bar{B} > 1.84$ for our example), the transition wave ceases to exist [inset (v)]. In this regime, frequency-invariant phonons cannot be induced from the outset, resulting in no energy harvesting potential.

For the maximum harvested energy, the lattice needs to be designed at the stable transition wave propagation limit. However, the increase in the harvesting performance with the lattice discreteness comes at the cost of reduced transport ability of the main transition waves. Figure 5(c) shows the nondimensionalized average propagation speed \bar{v}_{TW} of the transition waves between 30th and 49th sites, which decreases monotonically with the lattice discreteness. Each propagation speed is obtained by finding the zero crossings of the time responses at the 30th and 49th unit cells and dividing the physical distance between the unit cells by this time difference. The speed is then nondimensionalized with the multiplicative factor T/L. The stable transport ability of the bistable lattices is the core of generating the transducible phonons in the first place and the backbone of many extreme engineering applications [49, 50, 63, 76, 77]. Therefore, the lattice design needs to consider a balance between the extreme transport property and power conversion, depending on the desired functionalities.

In summary, our analysis reveals two performance gaps for input-independent energy harvesting from the induced phonons: the lower gap appears due to the negligibly small phonons, while the upper gap appears due to the breakdown of the transition wave itself. Between the gaps lies a pass band for topological wave energy harvesting, where the harvesting potential in general increases with the lattice discreteness level. The obtained performance diagrams provide a blueprint for designing multifunctional metamaterials with inherent energy harvesting capability.

7. Experimental response

We examine the experimental response of the model system to verify the invariance of the phonon frequency observed in the numerical analyses. We build an experimental bistable lattice by 3D-printing (Ultimaker 3 Extended) a ladder-like structure composed of 5 unit cells, as shown in Fig. 6(a). The CAD model with the key dimensions is provided in Appendix A. The rungs act as the on-site elements and are connected to their nearest neighbors through spring-shaped inter-site elements. A 15 g cube magnet is inserted at the center of each on-site element to serve as a mass. The magnets are arranged in an alternating NS-SN-NS-SN pattern to allow drastic changes in the magnetic fluxes through magnet coils (situated between the magnets) from their motion, which can be

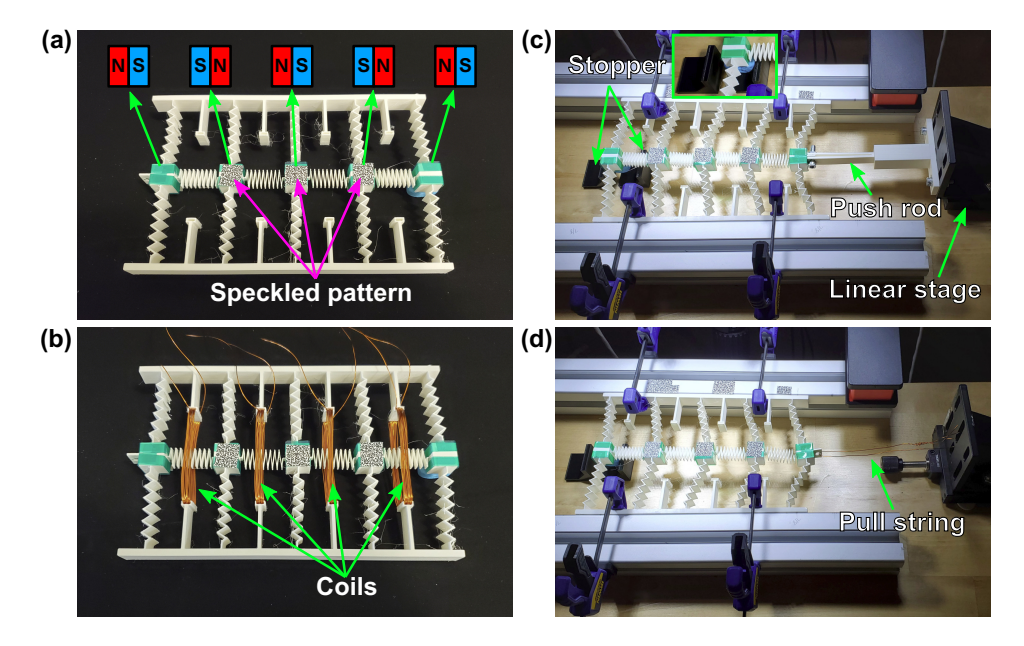


Figure 6. Experimental demonstrator for (a) DIC tests and (b) power generation tests. Experimental setups with the excitation mechanism for (c) compressive inputs and (d) tensile inputs.

later utilized for electromagnetic conversion (see Sec. 8). The bistability of each on-site element is achieved by precompressing the structure between two rails clamped to a laboratory table, and the stiffness of the on-site element is tuned by adding spring-like features on the rungs. The on-site elements are designed to be symmetric such that the stiffness values about the two stable equilibria are the same in the absence of other influences, such as the magnetic interaction or external load. As in the numerical analyses, a slight grading on the on-site potential is applied such that the first unit cell is compressed by 6.4 mm and the last unit cell is compressed by 0.8 mm to guarantee the transition waves propagation throughout the lattice. Also, a rubber stopper mechanism is implemented at the last (5th) unit cell to absorb large-amplitude overshoot from the free end, which is reflected and travels back in the opposite direction. Although the effect of these reflected waves cannot be completely suppressed by the stopper in our short lattice, their effect would not completely overshadow the crucial dynamics from the induced phonons in the metamaterial by the transition wave after the absorption.

To trigger a compressive transition wave, we displace the first element with a push rod at two different speeds, one quasi-statically and the other impulsively, by pulling and releasing a spring-loaded linear stage (THORLABS PT1B) impinging on the first element. Similar to Eq. (5), upon reaching the critical snapping distance, the push rod loses contact with the guide block fixed to the linear stage to allow spontaneous snap-through transition of the first unit cell [see Fig. 6(c) and Supplementary Video S1]. Similarly, to trigger a tensile transition wave, we pull the first element with a string of wire attached to the linear stage in the opposite direction to that of the compressive inputs. We use digital image correlation (DIC) to obtain the dynamic response of

individual unit cells experimentally. Pieces of adhesive paper with a random black-and-white speckled pattern are attached on top of the mass elements so that the image correlation software (VIC-3D) can track the displacements of the speckled regions [see Fig. 6(a)]. The displacements of the 2^{nd} unit cell in the direction of the lattice length are captured by two high-speed cameras (Photron UX100) with DSLR lenses (Nikon 24-85 mm f/2.8-4 D) at 1000 frames per second. We select the 2^{nd} unit cell so that the contribution from the reflected waves from the lattice end can be minimized.

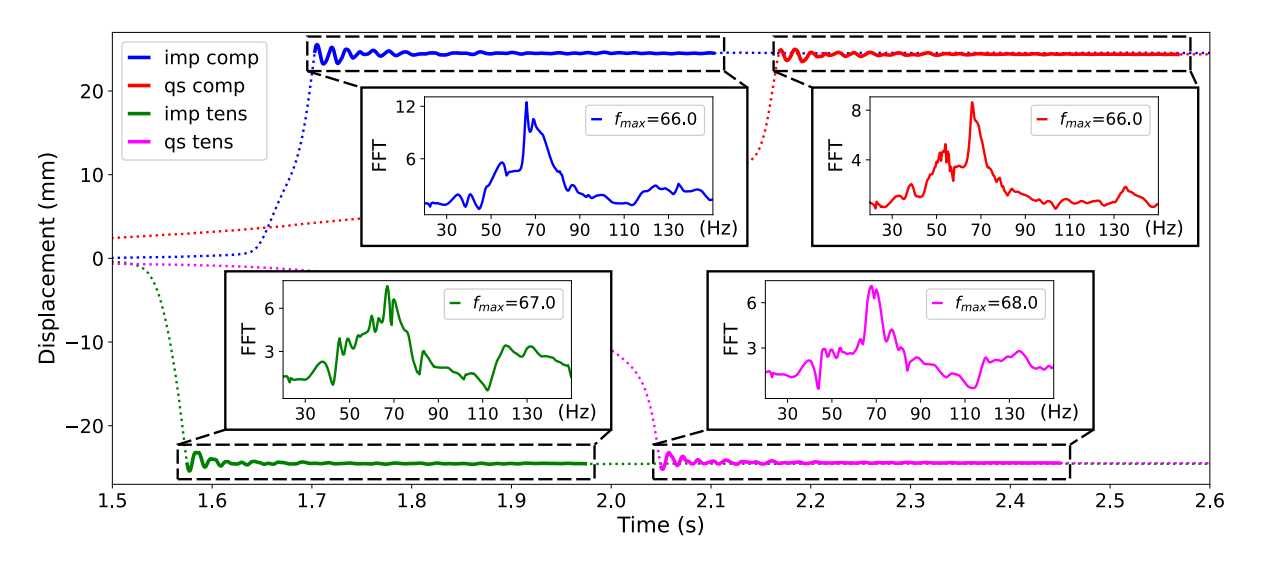


Figure 7. Time displacements of the 2nd unit cell obtained from the DIC under impulsive compressive (in blue), quasi-static compressive (in red), impulsive tensile (in green), and quasi-static tensile (in magenta) excitation, respectively. The solid curves indicate the tails induced by the transition wave. In the insets are the frequency spectra of the velocity corresponding to the tails.

Figure 7 shows the measured displacements of the 2nd unit cell under impulsive compressive, quasi-static compressive, impulsive tensile, and quasi-static tensile loads, respectively. Radiation of energy in the form of phonons following the snap-through transition is clearly noticeable as expected for a discrete bistable lattice and from the numerical simulations. The frequency spectra of the resulting phonons are obtained by the same technique described in Sec. 4 but for 2 s of the velocity data corresponding to the phonons at 1000 Hz sampling rate. The experimental observations are qualitatively in agreement with the simulated results: irrespective of the input conditions, the frequency response of the induced phonons at an internal unit cell shows that the dominant frequency peaks occur near a fixed value (66 Hz-68 Hz). The slight discrepancy in the dominant frequencies between the compressive and tensile input cases is mainly due to the magnetic influence, which tends to repulse the masses away from one another, resulting in asymmetry between the two stable equilibria. This asymmetry can be solved in real-world applications by introducing either a different power conversion mechanism, such as piezoelectric transduction, or a longer lattice, where the perturbations near the boundary become negligible in the length of the lattice.

Having the same dominant frequency outputs regardless of the excitation level and the propagation directions of the transition waves eliminates the need for separate or active circuit designs that need to be tuned to work optimally at varying frequencies. More generally, the response invariance breaks the connection between useful bandwidth and unit cell size impeding the broad implementation of energy harvesting, particularly for low-frequency vibration sources.

8. Topological wave energy conversion

To leverage the topological wave energy conversion afforded by the frequency-invariant phonons radiating from transition waves, we implement an electromagnetic induction mechanism for our resonant transduction. To demonstrate the conversion of the mechanical energy of the induced phonons to electrical energy, we place coils, each composed of 11 loops of 24-gauge copper wire, between neighboring magnets, where a large flux change is expected [see Fig. 6(b)]. The rate of change in magnetic flux through the coil induces an electric current, and the voltage across an electrical load $(R=1\ \Omega)$ is measured with a dSPACE data acquisition system (DS1104). Since the primary focus is on exploring the feasibility of the transducible signal generation, the specific choice of the coil design is not important as long as the electromagnetic interaction generates a large enough voltage to be detected by the data acquisition system. The voltage signals are amplified by 100 times with a signal amplifier (PCB 482A16) to obtain more distinguished voltage signals from the noise during the measurement.

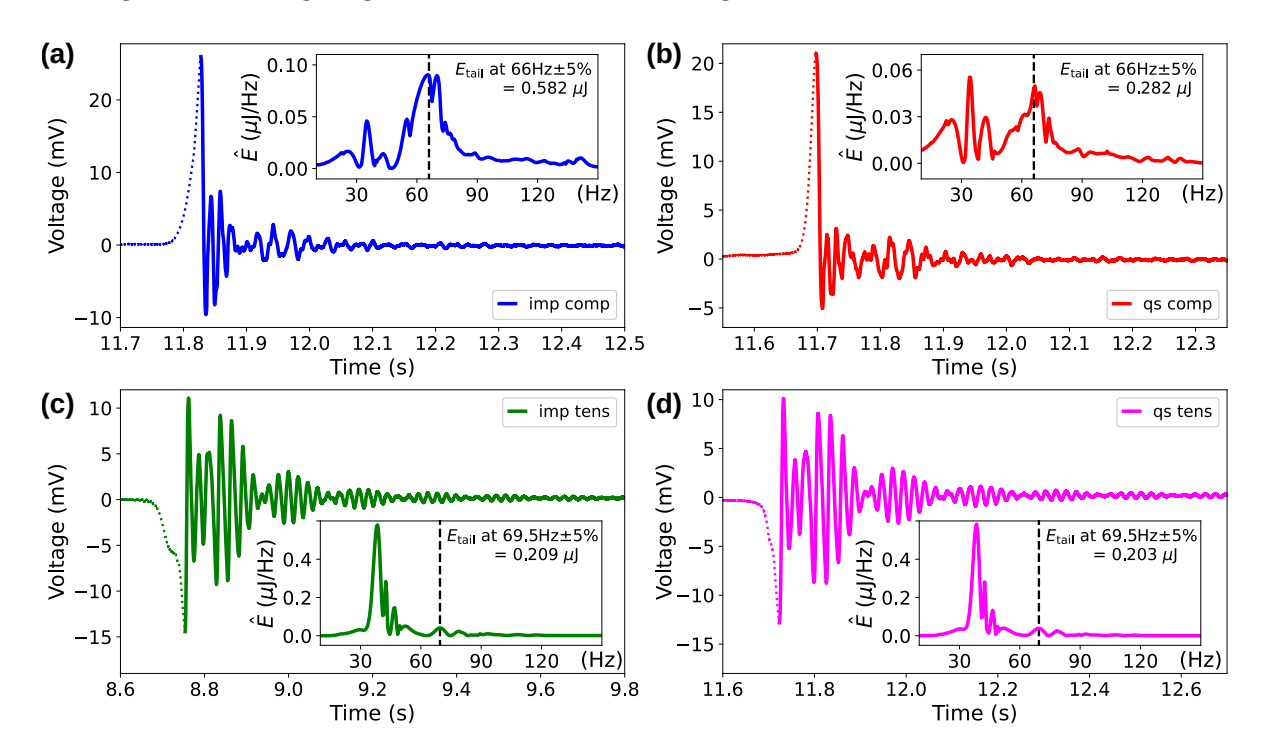


Figure 8. Voltage responses under (a) quasi-static compressive, (b) impulsive compressive, (c) quasi-static tensile, and (d) impulsive tensile inputs, respectively. In the insets are the corresponding energy spectral densities of the phonons.

Figure 8 shows the voltage responses obtained at the sites between the 2nd and 3rd elements, where the voltage signals are scaled back to the original unamplified levels. In the inset is the energy spectral density of the voltage response corresponding to the vibration trailing the transition wave. The energy spectral density is obtained by choosing $V/R^{1/2}$ as \hat{x}_n in Eq. (7) so that the right-hand side of the equation becomes an approximate transduced energy of the phonon at the measurement site.

Since the coil is situated between the 2nd and 3rd unit cells, the voltage response includes combined contributions from the motions of both unit cells. Ideally, the power conversion mechanism is better implemented exactly at the on-site element so that it mainly captures the motion of a single unit cell only. In our experimental system, the induced phonons' dominant frequencies vary between sites whereas their differences from the neighboring unit cells are not significant in our numerical simulations. Moreover, an implementation with no variation is difficult to achieve for our lattice design when using coils. This is due to the interference caused by the motion of the on-site element with the ideal placement of the coil. However, a different power conversion mechanism, such as a piezoelectric transducer, would help exploit the frequency-invariant phonons in full.

With the compressive transition waves, several frequency peaks appear consistently regardless of the intensity of the excitation triggering the transition waves. The energy peak at ~66 Hz corresponds to the frequency of the phonon induced by the transition wave. A group of low-frequency peaks (~25 Hz, ~35 Hz, and ~42 Hz) is attributed to the reflected waves from the boundary (see Appendix B). The peak at ~70 Hz is the second harmonic contribution of the ~35 Hz peak. This boundary effect cannot be eliminated in our 5-unit lattice, the manufacturing size of which is constrained by the build space of our 3D printer. Although these frequency peaks also occur input-independently, they would not be observed at the unit cells away from the boundary if the lattice were manufactured longer since the reflected waves would dissipate quickly in the length of the lattice. Accordingly, any contributions from these peaks will be disregarded in the remainder of the analyses.

The contribution from the 3rd unit cell (thus the boundary effect) is more substantial for the tensile transition waves since the 3rd unit cell vibrates much closer to the coil, in contrast to the compressive case. The peaks at 38.5 Hz and 46.5 Hz correspond to the reflected waves from the boundary (see Appendix B), the contribution of which would be minimized in a long lattice for the same reason as in the compressive transition wave case. Another peak at 42.5 Hz is deemed to be the dominant phonon frequency of the 3rd unit cell. This contribution would be minimized as well if the power conversion occurred at more ideal position (i.e., at the on-site element location). The direct contribution from the induced phonon at the 2nd unit cell remains as a small frequency peak at 69.5 Hz, which is invariant with respect to the input intensity. The peak frequency slightly differs from that of the compressive cases due to the asymmetric static equilibria as described in Sec. 7. In brief, we observe that the induced phonon has a nearly invariant frequency peak regardless of the intensity and direction of the input

excitations. Therefore, a transition wave can be considered as an excitation-independent generator of an oscillatory electrical source with a fixed frequency.

To assess the generated electrical energy that can be resonantly harvested, the available electrical energy within $\pm 5\%$ of the phonon frequency is measured. We apply different phonon frequencies for the compressive (66 Hz) and tensile (69.5 Hz) cases. However, in real applications, these frequencies should be tuned to be the same so that only a single tuned circuit would be needed. With our particular lattice, each propagation of a transition wave generates electrical energy ranging from 0.203-0.582 μ J at a unit cell. Since the response is obtained very close to the excitation site, the impulsive inputs tend to show greater electrical energy. However, the input energy would quickly dissipate in the first few unit cells in a long lattice [43], generating electrical energy at a comparable level independently of the input intensity. This result establishes that the radiated phonon from a transition wave can be converted into excitation-independent monochromatic electrical signals. Hence, we can achieve a robust energy harvesting mechanism without the need for any complicated circuit design to adapt to the changes in the input excitations.

9. Conclusion

We exploit the inherent discreteness of bistable lattices to achieve input-independent The discreteness allows the generation of phonons following energy harvesting. transition waves, where the most dominant frequency of the phonons at each unit cell occurs at a fixed frequency regardless of how the transition waves are generated. This invariance of the phonon frequencies implies that the radiated energy can always be efficiently harvested through resonant transduction. The lattice discreteness level can further control the energy harvesting potential, which, in general, increases with the discreteness as long as stable propagation of transition waves is ensured. With the integrated magnets and coils, we further confirm that the radiated phonon energy can be converted into electricity, the energy of which is concentrated around a fixed frequency at each unit cell, independent of the excitation nature. Thus, a transition wave acts as a generator of an input-independent electrical source (i.e., the induced phonon) with a fixed frequency, eliminating the need for any complicated electrical tuning devices to adapt to changes in the operating frequency. The proposed energy harvesting strategy effectively breaks the strong connection between the frequency bandwidth and the unit cell size intrinsic to the linear or weakly nonlinear metamaterials, hence addressing the existing challenges of broadband, particularly low-frequency, energy harvesting. Moreover, as long as the bistable lattice is discrete, the fundamental dynamics leading to the input-independent energy harvesting are scalable and material-independent, thus enabling the mechanism to be used in a wide variety of applications. The presented topological wave energy harvesting is inherent to generic lattices supporting transition waves, potentially enabling self-powered multifunctional metamaterials that can operate under broadband ambient sources.

Data availability statement

The data that support the findings of this study are available upon reasonable request from the authors.

Acknowledgments

The authors acknowledge the financial support from the National Science Foundation under grant CMMI-1935137.

Appendix A. CAD model

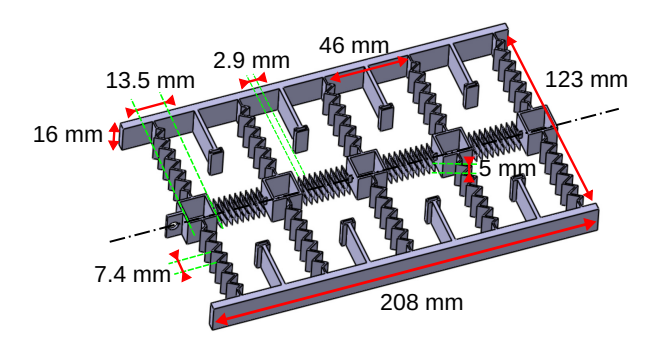


Figure A1. CAD model for the bistable lattice, showing key geometric dimensions.

Appendix B. Boundary effect

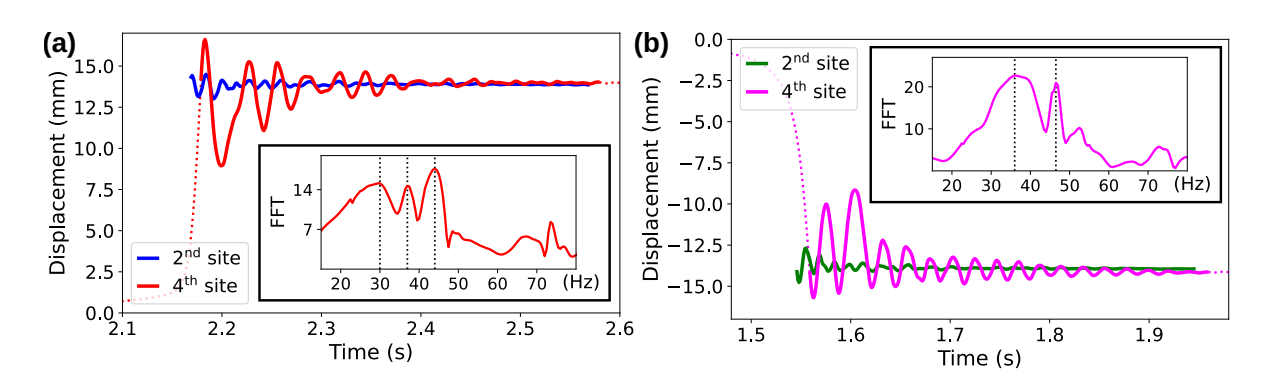


Figure B1. Displacements of the 4^{th} unit cell and their frequency spectra under (a) compressive and (b) tensile excitations. The displacements of the 2^{nd} unit cell are overlaid for an amplitude comparison.

The absorption mechanism at the 5th unit cell is implemented such that it allows the snap-through transition but prevents a significant overshoot in the snapping direction after the transition. Therefore, its response cannot be made identical to that of an infinite lattice unless the lattice is properly terminated [78], the practice of which is

nearly impossible to implement experimentally. Hence, large-amplitude responses at the unit cells near the boundary are unavoidable.

Figure B1 shows the displacements of the 4th unit cell under compressive and tensile inputs, respectively, and their frequency spectra. The induced vibration of the 2nd unit cell is plotted as well for an amplitude comparison. As expected, the response of the 4th unit cell has a much larger amplitude than that of the 2nd unit cell. The frequency spectrum of its velocity response under compressive input shows three low-frequency peaks (30 Hz, 37 Hz, and 44 Hz as indicated in dotted lines), which are deemed to result from the coupled vibrations of the boundary unit cells. Although the frequencies are slightly different, exactly the same cluster of frequency peaks can be observed in the voltage responses in Fig. 8(a,b). Thus, we interpret these low-frequency peaks as the reflection from the boundary, the contribution from which would be minimal at internal unit cells in a long lattice. Similarly, the contribution of the two peaks (36 Hz and 46.5 Hz) at the boundary appears in the voltage responses in Fig. 8(c,d) for the cases under tensile excitations.

References

- [1] S. Meninger, J.O. Mur-Miranda, R. Amirtharajah, A. Chandrakasan, and J.H. Lang. Vibration-to-electric energy conversion. *IEEE Transactions on Very Large Scale Integration (VLSI) Systems*, 9(1):64–76, February 2001. Conference Name: IEEE Transactions on Very Large Scale Integration (VLSI) Systems.
- [2] Shad Roundy, Paul K. Wright, and Jan Rabaey. A study of low level vibrations as a power source for wireless sensor nodes. *Computer Communications*, 26(11):1131–1144, July 2003.
- [3] Paul D. Mitcheson, Eric M. Yeatman, G. Kondala Rao, Andrew S. Holmes, and Tim C. Green. Energy Harvesting From Human and Machine Motion for Wireless Electronic Devices. Proceedings of the IEEE, 96(9):1457–1486, September 2008. Conference Name: Proceedings of the IEEE.
- [4] Chongfeng Wei and Xingjian Jing. A comprehensive review on vibration energy harvesting: Modelling and realization. Renewable and Sustainable Energy Reviews, 74:1–18, July 2017.
- [5] C. B. Williams and R. B. Yates. Analysis of a micro-electric generator for microsystems. *Sensors and Actuators A: Physical*, 52(1):8–11, March 1996.
- [6] H. A. Sodano, G. Park, and D. J. Inman. Estimation of Electric Charge Output for Piezoelectric Energy Harvesting. Strain, 40(2):49–58, 2004. Leprint: https://onlinelibrary.wiley.com/doi/pdf/10.1111/j.1475-1305.2004.00120.x.
- [7] N. G. Stephen. On energy harvesting from ambient vibration. *Journal of Sound and Vibration*, 293(1):409–425, May 2006.
- [8] F. Cottone, H. Vocca, and L. Gammaitoni. Nonlinear Energy Harvesting. *Physical Review Letters*, 102(8):080601, February 2009. Publisher: American Physical Society.
- [9] M. Ferrari, V. Ferrari, M. Guizzetti, B. Andò, S. Baglio, and C. Trigona. Improved energy harvesting from wideband vibrations by nonlinear piezoelectric converters. Sensors and Actuators A: Physical, 162(2):425–431, August 2010.
- [10] Pilkee Kim and Jongwon Seok. A multi-stable energy harvester: Dynamic modeling and bifurcation analysis. *Journal of Sound and Vibration*, 333(21):5525–5547, October 2014.
- [11] G. Scarselli, F. Nicassio, F. Pinto, F. Ciampa, O. Iervolino, and M. Meo. A novel bistable energy harvesting concept. *Smart Materials and Structures*, 25(5):055001, March 2016. Publisher: IOP Publishing.
- [12] NOËL E. DUTOIT, BRIAN L. WARDLE, and SANG-GOOK KIM. Design Consid-

- erations for Mems-Scale Piezoelectric Mechanical Vibration Energy Harvesters. *Integrated Ferroelectrics*, 71(1):121–160, July 2005. Publisher: Taylor & Francis Leprint: https://doi.org/10.1080/10584580590964574.
- [13] P. J. Cornwell, J. Goethal, J. Kowko, and M. Damianakis. Enhancing Power Harvesting using a Tuned Auxiliary Structure. *Journal of Intelligent Material Systems and Structures*, 16(10):825–834, October 2005. Publisher: SAGE Publications Ltd STM.
- [14] Eli S Leland and Paul K Wright. Resonance tuning of piezoelectric vibration energy scavenging generators using compressive axial preload. Smart Materials and Structures, 15(5):1413–1420, October 2006.
- [15] Vinod R. Challa, M. G. Prasad, Yong Shi, and Frank T. Fisher. A vibration energy harvesting device with bidirectional resonance frequency tunability. *Smart Materials and Structures*, 17(1):015035, January 2008. Publisher: IOP Publishing.
- [16] Joerg Schaufuss, Dirk Scheibner, and Jan Mehner. New approach of frequency tuning for kinetic energy harvesters. Sensors and Actuators A: Physical, 171(2):352–360, November 2011.
- [17] Wen-Jong Wu, Yu-Yin Chen, Bor-Shun Lee, Jyun-Jhang He, and Yen-Tun Peng. Tunable resonant frequency power harvesting devices. In *Smart Structures and Materials 2006: Damping and Isolation*, volume 6169, pages 55–62. SPIE, March 2006.
- [18] Christian Peters, Dominic Maurath, Wolfram Schock, Florian Mezger, and Yiannos Manoli. A closed-loop wide-range tunable mechanical resonator for energy harvesting systems. 19(9):094004, August 2009. Publisher: IOP Publishing.
- [19] Adrien Badel and Elie Lefeuvre. Wideband Piezoelectric Energy Harvester Tuned Through its Electronic Interface Circuit. 557:012115, November 2014. Publisher: IOP Publishing.
- [20] A. Morel, G. Pillonnet, P. Gasnier, E. Lefeuvre, and A. Badel. Frequency tuning of piezoelectric energy harvesters thanks to a short-circuit synchronous electric charge extraction. 28(2):025009, December 2018. Publisher: IOP Publishing.
- [21] E. L. Pradeesh and S. Udhayakumar. Effect of placement of piezoelectric material and proof mass on the performance of piezoelectric energy harvester. *Mechanical Systems and Signal Processing*, 130:664–676, September 2019.
- [22] E. L. Pradeesh, S. Udhayakumar, and C. Sathishkumar. Investigation on various beam geometries for piezoelectric energy harvester with two serially mounted piezoelectric materials. SN Applied Sciences, 1(12):1648, November 2019.
- [23] E. L. Pradeesh and S. Udhayakumar. Investigation on the geometry of beams for piezoelectric energy harvester. *Microsystem Technologies*, 25(9):3463–3475, September 2019.
- [24] Kota Mikoshiba, James M Manimala, and CT Sun. Energy harvesting using an array of multifunctional resonators. *Journal of Intelligent Material Systems and Structures*, 24(2):168–179, January 2013. Publisher: SAGE Publications Ltd STM.
- [25] M. Carrara, M. R. Cacan, M. J. Leamy, M. Ruzzene, and A. Erturk. Dramatic enhancement of structure-borne wave energy harvesting using an elliptical acoustic mirror. Applied Physics Letters, 100(20):204105, May 2012. Publisher: American Institute of Physics.
- [26] M. Carrara, M. R. Cacan, J. Toussaint, M. J. Leamy, M. Ruzzene, and A. Erturk. Metamaterial-inspired structures and concepts for elastoacoustic wave energy harvesting. Smart Materials and Structures, 22(6):065004, April 2013. Publisher: IOP Publishing.
- [27] Kaiyuan Li and Piervincenzo Rizzo. Energy harvesting using arrays of granular chains and solid rods. *Journal of Applied Physics*, 117(21):215101, June 2015. Publisher: American Institute of Physics.
- [28] Liang-Yu Wu, Lien-Wen Chen, and Chia-Ming Liu. Acoustic energy harvesting using resonant cavity of a sonic crystal. Applied Physics Letters, 95(1):013506, July 2009. Publisher: American Institute of Physics.
- [29] Hangyuan Lv, Xiaoyong Tian, Michael Yu Wang, and Dichen Li. Vibration energy harvesting using a phononic crystal with point defect states. Applied Physics Letters, 102(3):034103, January 2013. Publisher: American Institute of Physics.

- [30] Mourad Oudich and Yong Li. Tunable sub-wavelength acoustic energy harvesting with a metamaterial plate. *Journal of Physics D: Applied Physics*, 50(31):315104, July 2017. Publisher: IOP Publishing.
- [31] Arafa H. Aly, Ahmed Nagaty, Zaki Khalifa, and Ahmed Mehaney. The significance of temperature dependence on the piezoelectric energy harvesting by using a phononic crystal. *Journal of Applied Physics*, 123(18):185102, May 2018. Publisher: American Institute of Physics.
- [32] Jacopo M. De Ponti, Andrea Colombi, Raffaele Ardito, Francesco Braghin, Alberto Corigliano, and Richard V. Craster. Graded elastic metasurface for enhanced energy harvesting. New Journal of Physics, 22(1):013013, January 2020. Publisher: IOP Publishing.
- [33] Zhenkun Lin and Serife Tol. Elastic Metasurfaces for Full Wavefront Control and Low-Frequency Energy Harvesting. *Journal of Vibration and Acoustics*, 143(6), March 2021.
- [34] Gregory J. Chaplain, Jacopo M. De Ponti, Giulia Aguzzi, Andrea Colombi, and Richard V. Craster. Topological Rainbow Trapping for Elastic Energy Harvesting in Graded Su-Schrieffer-Heeger Systems. *Physical Review Applied*, 14(5):054035, November 2020. Publisher: American Physical Society.
- [35] M. F. Ashby. *Materials selection in mechanical design*. Butterworth-Heinemann, Burlington, MA, 4th ed edition, 2011. OCLC: ocn639573741.
- [36] Pierre A. Deymier. Introduction to Phononic Crystals and Acoustic Metamaterials. In Pierre A. Deymier, editor, *Acoustic Metamaterials and Phononic Crystals*, Springer Series in Solid-State Sciences, pages 1–12. Springer, Berlin, Heidelberg, 2013.
- [37] Zhengyou Liu, Xixiang Zhang, Yiwei Mao, Y. Y. Zhu, Zhiyu Yang, C. T. Chan, and Ping Sheng. Locally Resonant Sonic Materials. *Science*, 289(5485):1734, September 2000. 1734.
- [38] Haluk Kulah and Khalil Najafi. Energy Scavenging From Low-Frequency Vibrations by Using Frequency Up-Conversion for Wireless Sensor Applications. *IEEE Sensors Journal*, 8(3):261–268, March 2008. Conference Name: IEEE Sensors Journal.
- [39] Lei Gu and Carol Livermore. Impact-driven, frequency up-converting coupled vibration energy harvesting device for low frequency operation. *Smart Materials and Structures*, 20(4):045004, March 2011. Publisher: IOP Publishing.
- [40] Michele Pozzi. Impulse excitation of piezoelectric bimorphs for energy harvesting: a dimensionless model. *Smart Materials and Structures*, 23(4):045044, March 2014. Publisher: IOP Publishing.
- [41] Raj K. Narisetti, Michael J. Leamy, and Massimo Ruzzene. A Perturbation Approach for Predicting Wave Propagation in One-Dimensional Nonlinear Periodic Structures. *Journal of Vibration and Acoustics*, 132(3), April 2010.
- [42] R. Khajehtourian and M. I. Hussein. Dispersion characteristics of a nonlinear elastic metamaterial. AIP Advances, 4(12):124308, December 2014. Publisher: American Institute of Physics.
- [43] Myungwon Hwang and Andres F. Arrieta. Input-Independent Energy Harvesting in Bistable Lattices from Transition Waves. *Scientific Reports*, 8(1):3630, February 2018.
- [44] Myungwon Hwang and Andres F. Arrieta. Extreme Frequency Conversion from Soliton Resonant Interactions. *Physical Review Letters*, 126(7):073902, February 2021. Publisher: American Physical Society.
- [45] J. F. Currie, S. E. Trullinger, A. R. Bishop, and J. A. Krumhansl. Numerical simulation of sine-Gordon soliton dynamics in the presence of perturbations. *Physical Review B*, 15(12):5567–5580, June 1977. Publisher: American Physical Society.
- [46] Yuji Ishimori and Toyonori Munakata. Kink Dynamics in the Discrete Sine-Gordon System A Perturbational Approach. *Journal of the Physical Society of Japan*, 51(10):3367–3374, October 1982. Publisher: The Physical Society of Japan.
- [47] P. Woafo and T. C. Kofane. Kink dynamics in a discrete ϕ^4 chain with dissipation and external field. *Journal of Physics: Condensed Matter*, 5(38):7063–7074, September 1993. Publisher: IOP Publishing.
- [48] Neel Nadkarni, Chiara Daraio, and Dennis M. Kochmann. Dynamics of periodic mechanical structures containing bistable elastic elements: From elastic to solitary wave propagation.

- Physical Review E, 90(2):023204, August 2014. Publisher: American Physical Society.
- [49] Neel Nadkarni, Andres F. Arrieta, Christopher Chong, Dennis M. Kochmann, and Chiara Daraio. Unidirectional Transition Waves in Bistable Lattices. *Physical Review Letters*, 116(24):244501, June 2016. Publisher: American Physical Society.
- [50] Jordan R. Raney, Neel Nadkarni, Chiara Daraio, Dennis M. Kochmann, Jennifer A. Lewis, and Katia Bertoldi. Stable propagation of mechanical signals in soft media using stored elastic energy. *Proceedings of the National Academy of Sciences*, 113(35):9722–9727, August 2016.
- [51] Shmuel Katz and Sefi Givli. Solitary waves in a bistable lattice. Extreme Mechanics Letters, 22:106–111, July 2018.
- [52] L. I. Slepyan and M. V. Ayzenberg-Stepanenko. Localized transition waves in bistable-bond lattices. *Journal of the Mechanics and Physics of Solids*, 52(7):1447–1479, July 2004.
- [53] Julien Meaud. Multistable two-dimensional spring-mass lattices with tunable band gaps and wave directionality. *Journal of Sound and Vibration*, 434:44–62, November 2018.
- [54] Michel Remoissenet. Waves Called Solitons. Advanced Texts in Physics. Springer Berlin Heidelberg, Berlin, Heidelberg, 1999.
- [55] M. S. Kushwaha, P. Halevi, L. Dobrzynski, and B. Djafari-Rouhani. Acoustic band structure of periodic elastic composites. *Physical Review Letters*, 71(13):2022–2025, September 1993. Publisher: American Physical Society.
- [56] M. Sigalas and E. N. Economou. Band structure of elastic waves in two dimensional systems. Solid State Communications, 86(3):141–143, April 1993.
- [57] Mahmoud I. Hussein, Michael J. Leamy, and Massimo Ruzzene. Dynamics of Phononic Materials and Structures: Historical Origins, Recent Progress, and Future Outlook. Applied Mechanics Reviews, 66(4):040802, July 2014.
- [58] Michel Peyrard and Martin D. Kruskal. Kink dynamics in the highly discrete sine-Gordon system. *Physica D: Nonlinear Phenomena*, 14(1):88–102, December 1984.
- [59] Christian Kunz and J. Andrew Combs. Discrete theory of kink diffusion in the ϕ^4 lattice with comparison to the continuum approximation. *Physical Review B*, 31(1):527–535, January 1985. Publisher: American Physical Society.
- [60] Herre S. J. van der Zant, Terry P. Orlando, Shinya Watanabe, and Steven H. Strogatz. Kink Propagation in a Highly Discrete System: Observation of Phase Locking to Linear Waves. Physical Review Letters, 74(1):174–177, January 1995. Publisher: American Physical Society.
- [61] Myungwon Hwang and Andres F. Arrieta. Energy harvesting characteristics in metamaterials based on bistable lattices. In Active and Passive Smart Structures and Integrated Systems XIII, volume 10967, page 109670B. International Society for Optics and Photonics, March 2019.
- [62] A. Carpio and L. L. Bonilla. Oscillatory wave fronts in chains of coupled nonlinear oscillators. *Physical Review E*, 67(5):056621, May 2003. Publisher: American Physical Society.
- [63] Lishuai Jin, Romik Khajehtourian, Jochen Mueller, Ahmad Rafsanjani, Vincent Tournat, Katia Bertoldi, and Dennis M. Kochmann. Guided transition waves in multistable mechanical metamaterials. Proceedings of the National Academy of Sciences, 117(5):2319–2325, February 2020.
- [64] Romik Khajehtourian and Dennis M. Kochmann. Soft Adaptive Mechanical Metamaterials. *Frontiers in Robotics and AI*, 8, 2021. Publisher: Frontiers.
- [65] Myungwon Hwang and Andres F. Arrieta. Solitary waves in bistable lattices with stiffness grading: Augmenting propagation control. *Physical Review E*, 98(4):042205, October 2018. Publisher: American Physical Society.
- [66] Vinod Ramakrishnan and Michael J. Frazier. Transition waves in multi-stable metamaterials with space-time modulated potentials. Applied Physics Letters, 117(15):151901, October 2020. Publisher: American Institute of Physics.
- [67] Myungwon Hwang, Carlo Scalo, and Andres F. Arrieta. High-performance large-scale simulation of multi-stable metastructures. *In Review*.
- [68] David Restrepo, Nilesh D. Mankame, and Pablo D. Zavattieri. Phase transforming cellular

- materials. Extreme Mechanics Letters, 4:52–60, September 2015.
- [69] Nikolaos Vasios, Bolei Deng, Benjamin Gorissen, and Katia Bertoldi. Universally bistable shells with nonzero Gaussian curvature for two-way transition waves. Nature Communications, 12(1):695, December 2021.
- [70] Lauren C. Montemayor, Lucas R. Meza, and Julia R. Greer. Design and Fabrication of Hollow Rigid Nanolattices via Two-Photon Lithography. *Advanced Engineering Materials*, 16(2):184–189, 2014. _eprint: https://onlinelibrary.wiley.com/doi/pdf/10.1002/adem.201300254.
- [71] Sebastian Krödel and Chiara Daraio. Microlattice Metamaterials for Tailoring Ultrasonic Transmission with Elastoacoustic Hybridization. *Physical Review Applied*, 6(6):064005, December 2016. Publisher: American Physical Society.
- [72] Jingyuan Qu, Muamer Kadic, Andreas Naber, and Martin Wegener. Micro-Structured Two-Component 3D Metamaterials with Negative Thermal-Expansion Coefficient from Positive Constituents. Scientific Reports, 7(1):40643, January 2017. Bandiera_abtest: a Cc_license_type: cc_by Cg_type: Nature Research Journals Number: 1 Primary_atype: Research Publisher: Nature Publishing Group Subject_term: Composites; Mechanical properties Subject_term_id: composites; mechanical-properties.
- [73] Yuanping Song, Robert M. Panas, Samira Chizari, Lucas A. Shaw, Julie A. Jackson, Jonathan B. Hopkins, and Andrew J. Pascall. Additively manufacturable micro-mechanical logic gates. Nature Communications, 10(1):882, February 2019. Bandiera_abtest: a Cc_license_type: cc_by Cg_type: Nature Research Journals Number: 1 Primary_atype: Research Publisher: Nature Publishing Group Subject_term: Mechanical engineering;Sensors Subject_term_id: mechanical-engineering;sensors.
- [74] R. Hobart. Peierls Barrier Analysis. Journal of Applied Physics, 37(9):3573–3576, August 1966. Publisher: American Institute of Physics.
- [75] Oleg M. Braun and Yuri S. Kivshar. Nonlinear dynamics of the Frenkel–Kontorova model. *Physics Reports*, 306(1):1–108, December 1998.
- [76] H. Yasuda, L. M. Korpas, and J. R. Raney. Transition Waves and Formation of Domain Walls in Multistable Mechanical Metamaterials. *Physical Review Applied*, 13(5):054067, May 2020. Publisher: American Physical Society.
- [77] Ahmad Zareei, Bolei Deng, and Katia Bertoldi. Harnessing transition waves to realize deployable structures. *Proceedings of the National Academy of Sciences*, 117(8):4015–4020, February 2020.
- [78] Iain G. Main. Vibrations and Waves in Physics. Cambridge University Press, Cambridge, 1993.